geosciences

MDPI

Article

Echo Sounding for Remote Estimation of Seabed Temperatures on the Arctic Shelf

Vladimir Yusupov [1,2,*], Aleksandr Salomatin [3], Natalia Shakhova [1,3], Denis Chernykh [1,3], Anna Domaniuk [3] and Igor Semiletov [1,3]

[1] Laboratory of the Arctic land shelf interaction, Tomsk State University, 634050 Tomsk, Russia
[2] Federal Scientific Research Center "Crystallography and Photonics" RAS, Institute of Photon Technologies, 108840 Moscow, Russia
[3] V.I. Ilyichev Pacific Oceanological Institute, Far Eastern Branch of the Russian Academy of Sciences, 690041 Vladivostok, Russia
* Correspondence: iouss@yandex.ru

Abstract: The East Siberian Arctic Shelf (ESAS) is a key area of CH_4 venting in the Arctic Ocean. The ESAS region stores more than 80% of the world's predicted subsea permafrost and associated permafrost-related gas hydrates. Gas emissions from subsea permafrost are controlled by its current thermal state, which, in turn, depends on environmental factors. The aim of the manuscript is to show that the thermal state of subsea permafrost and phase transitions of its pore moisture can be estimated remotely by echo soundings, which can resolve the structure of shallow bottom sediments. It has been found that the duration of the seabed acoustic response (echo duration, Δ) at frequencies of 50 and 200 kHz correlates with sediment temperatures and generally increases with cooling below 0.5 °C. This correlation, explained by assuming a layered structure of the bottom sediments, establishes the basis for high-frequency acoustic thermometry. The technique is an advantageous tool for many applications: fast contouring of low-temperature zones, remote measurements of seabed surface temperature, and estimation of the thickness of frozen sediments near the bottom. The latter estimates have implications for the distribution of subsea permafrost and the stability of gas hydrates on the Arctic shelf.

Keywords: sound penetration; attenuation; subsea permafrost; seabed temperature; methane release; East Siberian Arctic Shelf

Citation: Yusupov, V.; Salomatin, A.; Shakhova, N.; Chernykh, D.; Domaniuk, A.; Semiletov, I. Echo Sounding for Remote Estimation of Seabed Temperatures on the Arctic Shelf. *Geosciences* **2022**, *12*, 315. https://doi.org/10.3390/geosciences12090315

Academic Editors: Jesús Ruiz-Fernández and Jesus Martinez-Frias

Received: 3 July 2022
Accepted: 22 August 2022
Published: 25 August 2022

1. Introduction

The Arctic is warming dramatically, with potentially catastrophic impacts on the climate through rapid mobilization of the reservoirs of carbon sequestered in permafrost [1]. Thawing permafrost in the Arctic is the major contributing factor to the transportation of substantial amounts of carbon from land and ocean to the atmosphere on decadal–century timescales [2–4]. One possible effect is the release of previously generated methane (CH_4) preserved within seabed deposits, such as natural gas fields and coal beds, and the collapse of the CH_4 hydrates underlying the Arctic seabed [5,6]. The East Siberian Arctic Shelf (ESAS) is a key area of CH_4 venting in the Arctic Ocean. The ESAS region, which covers over two million square kilometers (equal to the areas of Germany, France, Great Britain, Italy, and Japan combined), stores over 80% of the world's predicted subsea permafrost and permafrost-related hydrates. This vast yet shallow region is a significant modern source of atmospheric CH_4, with annual contributions no less than those from terrestrial Arctic ecosystems [7,8]. However, unlike terrestrial ecosystems, ESAS emits CH_4 year-round due to its partial openness during the winter when terrestrial ecosystems are dormant [9]. Emissions are determined by and dependent on the current thermal state of the subsea permafrost and environmental factors controlling its dynamics [7–10]. A potential of 1400 Gt CH_4, in the form of hydrates, free gas, and organic carbon preserved

in the ESAS seabed, can be released into the water-atmosphere system in the form of CH_4 bubbles [7–9,11].

Temperature and pressure conditions in wide areas of the seafloor allow subsea methane accumulation in the form of gas hydrates, which might decay if disturbed. The estimated total amount of methane-bearing sediments in the offshore Arctic Basin amounts to 10^{15} m^{-3} (540 Gt of carbon) [6]. A potential of 1400 Gt CH_4, in the form of hydrates, free gas, and organic carbon preserved in the ESAS seabed, can become a substrate for anaerobic production in situ [5,9]. The current atmospheric CH_4 burden is ~5 Gt C–CH_4. Therefore, small changes in the current carbon stock of the subsea methane hydrate system might significantly affect the growth of CH_4 in the Arctic/Subarctic atmosphere. It might be a possible mechanism of maximum methane formation over the Arctic [7,9] -allowing another different perspective on the role of the Arctic Ocean as a source of methane emission to the global atmosphere. Once started, methane release from hydrates in the shallow Arctic shelf can trigger further climate impacts.

The effect of climate change on the subsea permafrost–hydrate system is often studied by means of modeling. However, the modeling approach has many limitations, including the dynamics of the water surface–sediment thermal equilibration and limited opportunity for validation against borehole temperature logs [12–14]. On the other hand, the area is poorly accessible for direct measurements of sediment surface temperatures, which remain sporadic [15]. In this respect, remote sensing of seabed temperatures from research vessels, at stations or while cruising, is of crucial importance.

The purpose of the article is to show that the seabed temperatures can be estimated remotely using acoustic methods. Acoustic methods are an efficient tool for marine research and have been used broadly. The reason is that the attenuation of acoustic waves propagating through the sea is lower than in any other type of soundings. Many acoustic oceanographic methods based on backscattering are used successfully to study the seafloor and gas emanations [16–20]. Such soundings enhance the performance of exploration and experimental work and significantly extend the scope of research objectives. Various sonar systems allow classifying bottom sediments [21] and mapping the seabed topography [22,23]. Echo sounding has applications in numerous fields: fishery, seafood production, petroleum production (tracing cuttings dispersed from drill holes or oil spills), sea flora monitoring, geological engineering surveys, cable and pipeline lining, dredging, mineral and petroleum exploration, navigation safety, construction in shelf and coastal areas, etc.

Field, laboratory, and theoretical data collected in this study demonstrate that the thermal state of surface sediment/subsea permafrost and its phase transitions can be estimated remotely with standard onboard sonar systems.

2. Materials and Methods

The acoustic surveys were performed during the Trans-Arctic cruise of research vessel (*RV) Nikolay Kolomeitsev* in August–September 2000 at forty-three stations in the East Siberian Sea and Laptev Sea shelf areas, as well in the Anadyr Gulf (Bering Sea), at sea depths ranging from 5 to 92 m. The soundings were run using a portable dual-frequency Furuno sonar system (Nagasaki, Japan) at 50 and 200 kHz, beam halfwidths of 12° and 2.5°, respectively, and a pulse length of 1 ms. Ultrasonic signals from transducers at a depth of 2–3 m were transmitted and received in the vertical plane. The main specifications of the acoustic system are summarized in Table 1.

While cruising, acoustic data were acquired by a high-performance Atlas echo sounder (Bremen, Germany) at a frequency of 210 kHz and a beam halfwidth of 4°. Measurements with the Furuno echo sounder (50 and 200 kHz) were carried out only at stations and with the Atlas echo sounder (210 kHz) only while the ship was moving. This made it possible to avoid aliasing in signals of the two used echo systems.

The reflection coefficient of acoustic waves from the seabed was estimated as in [24]. The duration Δ (ms) of echo signals backscattered from the upper layer of bottom sediments

was estimated from the averaged backscatter echo signal after subtracting the noise and eliminating the effect of the ship's roll. This duration Δ (ms) was equal to the time interval from the beginning of the seabed echo signal to the boundary below in which the signal amplitude does not exceed 2% (threshold) of its maximum value.

Table 1. The main specifications of the Furuno sonar system.

Parameter	Channel 1	Channel 2
Operating frequencies, kHz	50	200
Beam halfwidth, °	12.5	2.5
Peak power, W	200	100
Pulse length, ms	0.5; 1; 3; 10	0.5; 1; 3; 10

The measurements at stations included seawater and bottom sediment temperatures and sediment grain sizes. Water temperature profiles were measured through the water column from 2 to 3 m below the sea surface to the bottom surface using the standard Alec Electronics CTD probe (Kobe, Japan) with an accuracy of 0.05 °C. Sediments for particle size analysis were sampled using a Van Veen grab sampler (Silkeborg, Denmark). Bottom sediment temperatures were measured to a precision of 0.1 °C using four thermal sensors installed 50 cm apart along a 2 m steel rod [25] embedded 1 m into bottom sediments on average. The sediment temperature gradient was estimated as the difference between temperatures at 1 m depth and near the surface.

The data are quoted as average values with standard deviation. The significance of the difference between variable values was checked using the Wilcoxon signed-rank non-parametric statistical test.

3. Results and Discussion

3.1. Acoustic and Direct Measurements of Bottom Sediment Temperatures on the Russian Arctic Shelf and Comparisons

Acoustic responses acquired while cruising showed mainly plain bottom surface topography along the whole ship track within the East Siberian Arctic shelf.

However, significant sea depth variations were observed at a few local sites, such as a site in the Laptev Sea shelf (Figure 1a), where sea depths vary markedly though increasing in general. The seabed at the site mainly dips at 0.02° and reaches a dip of 5° in the steepest zones (curve 1 in Figure 1b). The reflection coefficient (curve 2 in Figure 1b) ranges from ~0 to 0.054 (0.026 ± 0.009 on average). The sporadic reflection went down to almost zero due to sediment gas saturation—an effect well-known as the blanking zone [14].

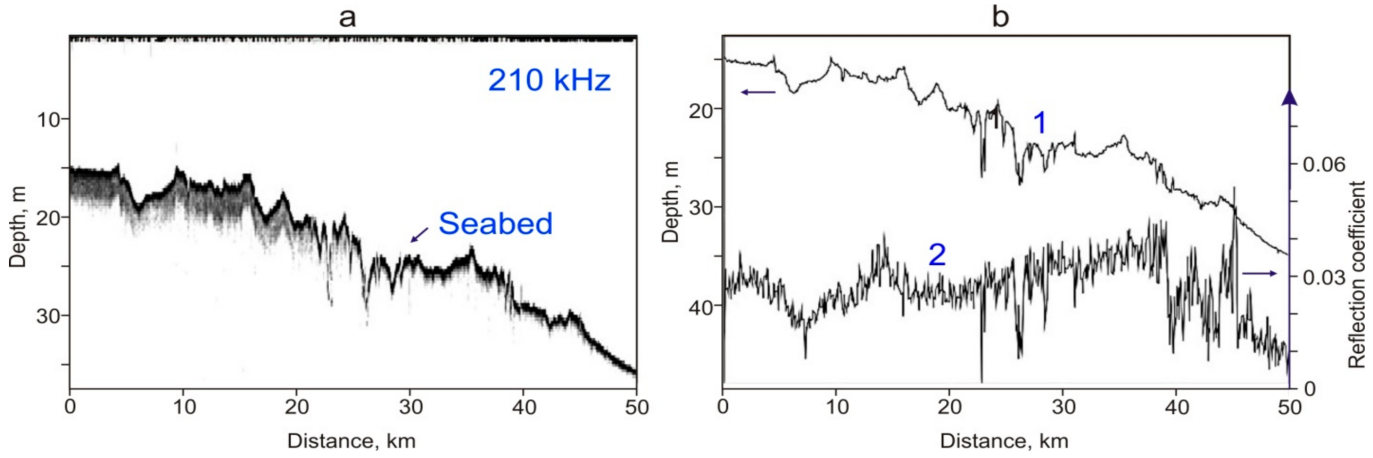

Figure 1. Example echograms along a profile in the Laptev Sea, in a zone of variable sea depths (**a**), frequency 210 kHz; curves in panel (**b**) are sea depths (1) and acoustic reflection (2).

Figure 2 shows fragments of typical echograms at 50 and 200 kHz acquired during drift at a station in the Laptev Sea. The vertical scale on the left shows the depth, and on the right, the time interval after the generation of the acoustic pulse. The water temperature profile (Figure 2a) comprises two quasi-homogeneous segments (near the water surface and near the seabed) and a layer of quite a high gradient between them, at sea depths from 40 to 55 m. Echograms (Figure 2a) and an averaged acoustic profile (Figure 2b) image segments of strong backscattering associated with the water surface and seabed, and a scattering layer of possible biological origin detectable at high frequencies at sea depths of 20–30 m.

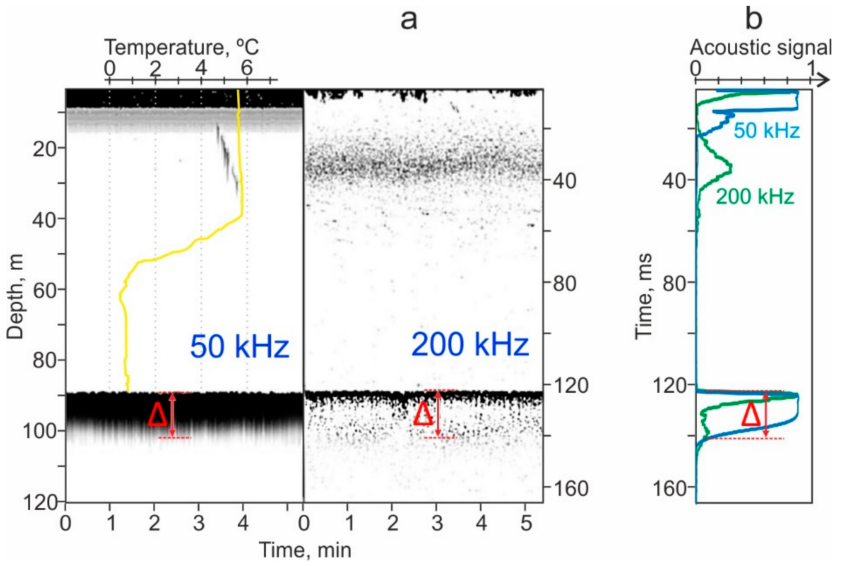

Figure 2. An example of acoustic signal registration at a station in the Laptev Sea at frequencies of 50 and 200 kHz. (**a**) Echograms with the registration of the seabed. The yellow curve shows the temperature profile. (**b**) View of two acoustic signals (in arbitrary units) at different frequencies. Red arrows show the duration of the echo signal backscattered from the seabed Δ.

Temperature estimation by the acoustic method that we suggest is based on the duration of acoustic signals backscattered from the seabed or echo duration Δ (red arrows in Figure 2). Such duration can be measured in meters, assuming that the sound speed in sediments corresponds to that in the water, or more correctly, in milliseconds.

Echo durations Δ, according to data from all stations, recorded at both frequencies (Figure 3), ranged from 1 to 19 ms. The values Δ > 4 ms can be classified as anomalously high since such values were not observed by us in more southern regions of the world ocean at such frequencies. Such anomalously high Δ values were recorded at quite a few stations along the whole ship track (open blue circles in Figure 3).

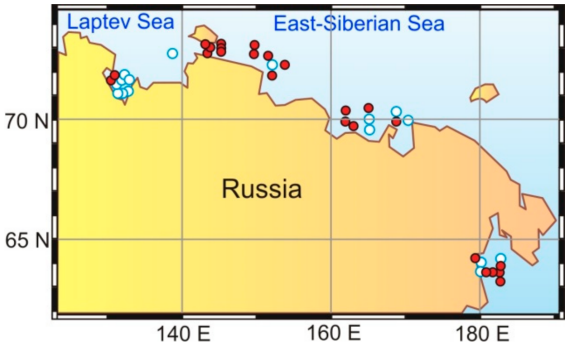

Figure 3. Location of stations on the Russian Arctic shelf (circles). Open blue circles are stations where anomalous echo durations (Δ > 4 ms) were recorded.

Comparison with the temperature data of the upper layer of sediments at a depth of 1 m showed that almost all cases with an anomalous duration of acoustical signals from the seabed correspond to negative temperatures. As can be seen from the fragments of the echograms shown in Figure 4, at positive temperatures, $\Delta < 5$ ms for a frequency of 50 kHz and $\Delta < 4$ ms for 200 kHz, while at negative temperatures, these values are much larger and reach $\Delta = 20$ ms.

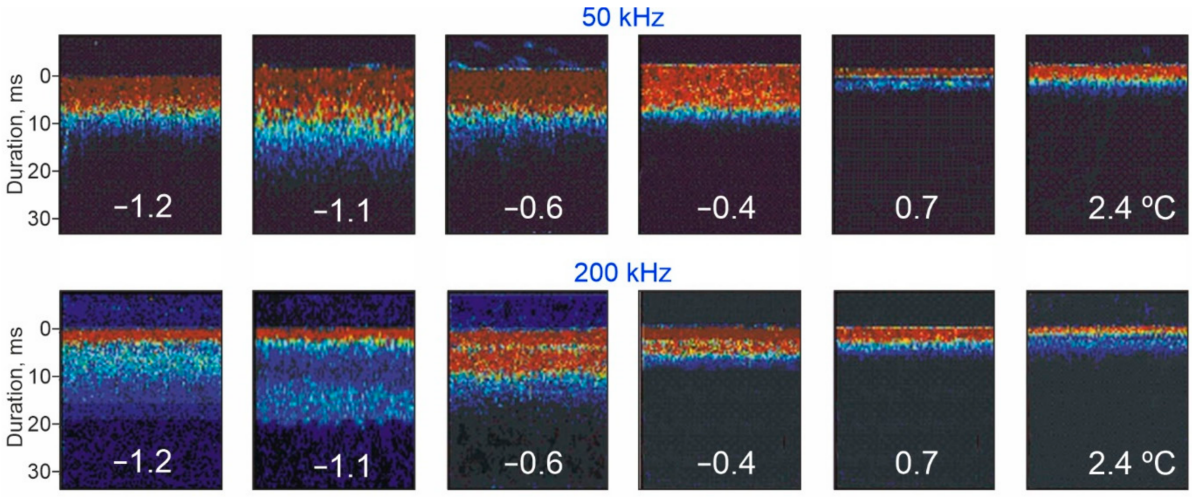

Figure 4. Fragments of echograms, 50 and 200 kHz. Echo duration (y axis) at different sediment temperatures at 1 m sediment depth (white numerals).

Figure 5 represents the values of Δ for all stations: it can be seen that in the sediment of positive temperatures, the duration's Δ for both frequencies depends weakly on temperature. However, in the region of negative temperatures, $\Delta > 4$ ms and, on average, increases quite rapidly with decreasing temperature. Thus, the areas with negative and positive temperatures of the upper layer of sediments differ significantly from each other both in duration Δ and in temperature dependence Δ.

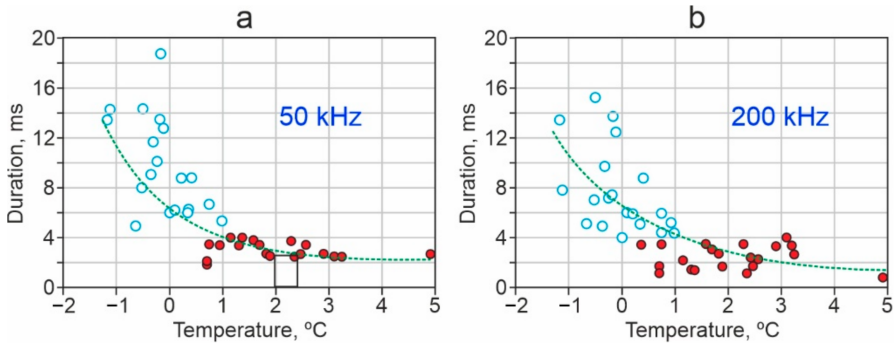

Figure 5. Temperature dependence of echo duration, 50 kHz (**a**) and 200 kHz (**b**). Open blue circles refer to stations where ultrasound penetrated anomalously deep into sediments. Dotted lines show general trends.

The statistical significance of the difference between Δ values at positive and negative temperatures was checked using the Wilcoxon test for the medians of echo duration series in the $T < T_0$ and $T > T_0$ regions and was the highest at $T_0 = 0.5$ °C. The probability of a zero hypothesis (meaning that the median Δ values for the two regions would not differ significantly) was as low as 2×10^{-7} for 50 kHz and 8×10^{-7} for 200 kHz.

At the next step, the low- and high-frequency echo durations Δ were correlated with temperature gradients in the upper 1 m of bottom sediments (Figure 6). The Δ values were the largest in areas of high negative temperature gradients (rapid depthward cooling of

sediments). Average gradients corresponding to $\Delta > 4$ ms were -0.6 ± 0.6 °C/m for 50 kHz and -0.5 ± 0.6 °C/m for 200 kHz. Note that the sediment temperature gradient, which ranged from −1.1 to +0.9 °C/m, is correlated with both large and small Δ (above and below 4 ms). The echo durations are anomalous ($\Delta > 4$ ms) for both frequencies only at stations where values of the negative temperature gradients were the highest (−1.7 to −1.5 °C/m).

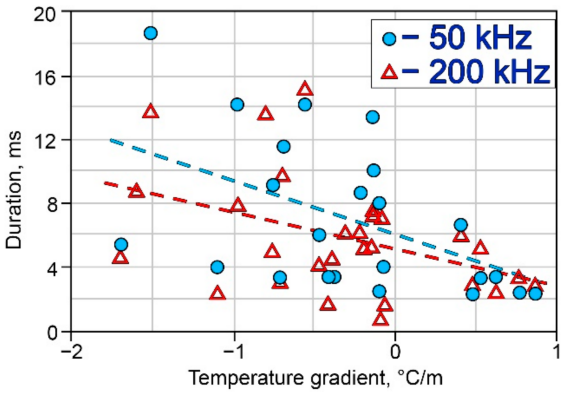

Figure 6. Echo duration vs. temperature gradient in upper 1 m of bottom sediments, 50 kHz (bold blue circle) and 200 kHz (open red triangles). Dotted lines show linear trends.

Particle size analysis of shallow bottom sediments sampled at stations revealed variations from 0.01 to 1.0 mm. The grain sizes correlate with acoustic data (Δ) at stations with sediment temperatures $T_0 = 0.5$ °C or higher (Δ decrease generally as grain sizes increase), but no correlation is observed at stations where the sediments are colder than $T_0 = 0.5$ °C.

Thus, the low- and high-frequency echo duration Δ mainly correlates with the temperature of the upper layer of sediments within the shallow Arctic shelf and generally increases as the temperatures decrease at temperatures of sediment $T < T_0 = 0.5$ °C.

3.2. Correlation of Echo Duration with Sediment Surface Temperatures: Modeling Approach

An analysis of 50 and 200 kHz acoustic data revealed anomalous echo duration values of >4 ms, up to 20 ms, at some sites of the Arctic shelf (Figure 5). Such Δ values are hardly due to scattering on the bottom surface but rather may result from signal penetration into sediments and volume scattering. Indeed, the layer corresponding to surface scattering and the side beam lobe (200 kHz) is located at a depth of 1 ms even at the maximum 92 m sea depth. As for the lower frequency (50 kHz), the layer corresponding to surface scattering and the main beam lobe is within 4 ms for most of the shallow-water stations (≤40 m).

Almost all sites of >4 ms echo duration correlate with zones of negative sediment temperatures, and the responses of progressively colder sediments become ever longer on average (Figure 5). A fairly clear dependence is registered (Figure 5): with a decrease in these temperatures, the duration of the echo signal Δ increases on average.

This correlation may be explained as follows. The echo duration Δ has two main controls: reflection from heterogeneities (commonly layered features) and attenuation in sediments. Namely, Δ is greater at higher reflection coefficients and lower attenuation.

3.2.1. Temperature Dependence of the Ultrasonic Reflection Coefficient on the Layered Structure

Let us first consider the temperature dependence of the ultrasonic reflection coefficient on the layered structure. The reflection coefficient from an ideal interface between two quasi-homogeneous layers is determined by the acoustic impedance (AI) jump [26], and its temperature dependence is sensitive to lithology. However, real interfaces commonly include an intermediate layer with a nonzero thickness and roughness. Backscattering from such a feature depends on the ratio of interface parameters (rms roughness height σ and effective thickness of the intermediate layer) to the wavelength [27]. The wavelengths and reflection coefficients are greater in frozen sediments, where the sound has a greater

speed. Specifically, when sediments freeze, due to an increase in the speed of sound, the wavelength will increase, so the reflection will increase too.

In addition to the acoustic impedance, the reflection coefficient of acoustic waves from a rough surface (V) depends on the Rayleigh roughness criterion $P = 4\pi\sigma/\lambda$, where λ is the wavelength [28]:

$$V = V_0 \cdot \exp\left(-P^2/2\right), \quad (1)$$

V_0 in (1) is the reflection coefficient for an ideally smooth interface. The frequency dependence of a normalized reflection coefficient of a normal incident acoustic wave from a sand layer with different roughness values σ is plotted in Figure 7. At very low frequencies <3 kHz, the interface is almost ideal, and the roughness does not affect the reflection coefficient, but reflection from a rough interface at >1 MHz reduces almost to zero.

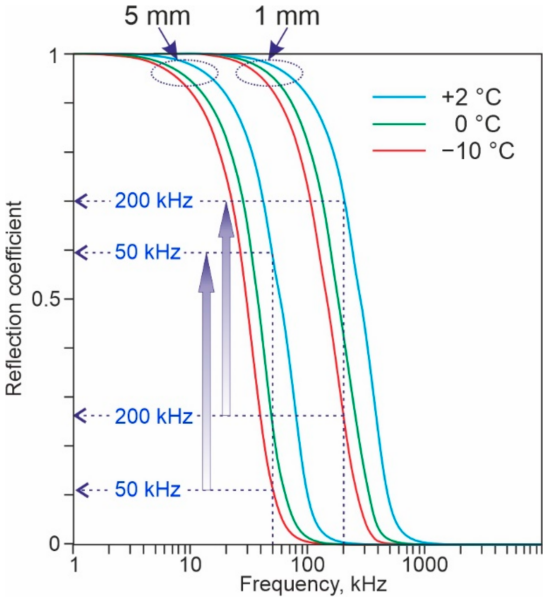

Figure 7. Frequency dependence of a normalized reflection coefficient from a rough sandstone surface, calculated for temperatures of 2 °C (1), 0 °C (2) and −10 °C (3) and roughness heights of 1 and 5 mm. The vertical violet arrows show roughness-related reflection coefficient increase as the sand cools down from +2 to −10 °C.

Figure 7 shows that each value of the roughness parameter has its own frequency range, for which the temperature dependence of V is most pronounced. Therefore, when a sandstone layer cools from +2 to −10 °C, the reflection coefficient increases especially rapidly at σ = 5 mm between 30 and 100 kHz but at σ = 1 mm in the 150–400 kHz range: approximately from 0.1 to 0.6 at 50 kHz and σ = 5 mm roughness and from 0.27 to 0.7 at 200 kHz and σ = 1 mm.

In order to estimate the coefficient of reflection from the transitional layer of a nonzero thickness, the respective real jump in the speed of sound in the transition layer Δc is approximated by the first-order Epstein function [28] (Figure 8a)

$$c(z) = c_0 \cdot \left(1 - \frac{\Delta c}{c} \cdot \frac{\exp(mH)}{1 + \exp(mH)}\right)^{-1/2}, \quad (2)$$

where H is the depth (H = 0 in the middle of the intermediate layer), and the parameter m is determined by the effective thickness of the intermediate layer. $m = 4/\Delta h$ at the effective thickness

$$\Delta h = \frac{\Delta c}{dc/dH_{H=0}}, \quad (3)$$

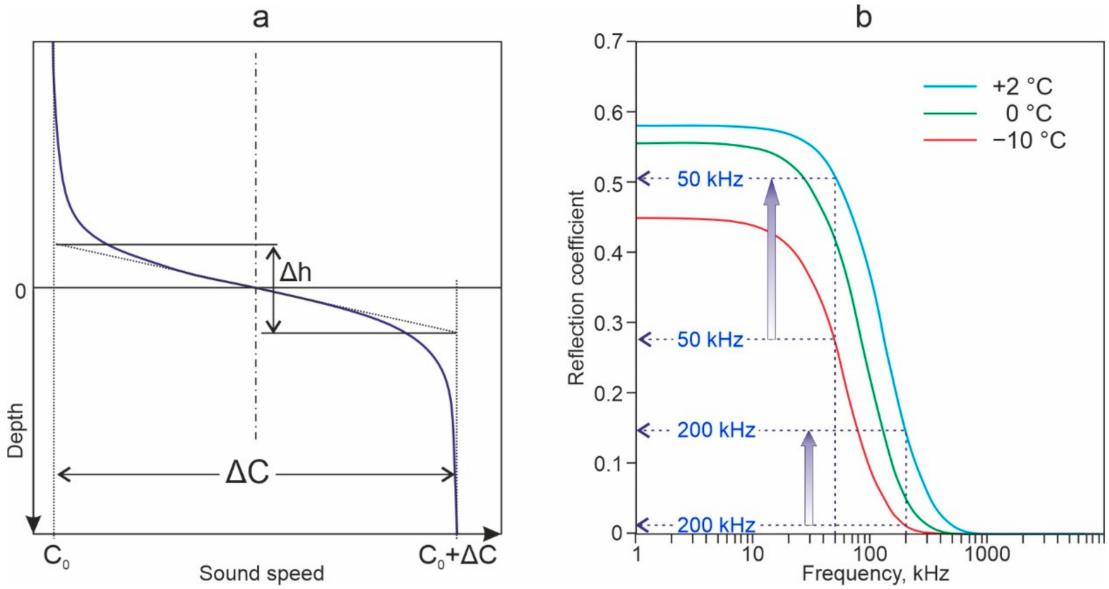

Figure 8. (**a**) Boundary between two homogeneous layers as an Epstein transition layer with a thickness Δh; (**b**): frequency dependence of reflection from the sand–clay interface as an Epstein transition layer with = 10 mm at temperatures +2 °C (1), 0 °C (2), and −10 °C (3). Violet arrows show a reflection coefficient increase from +2 °C to −10 °C cooling of the 10 mm thick interface.

This approximation describes real transition layers quite well and allows an ana-lytical solution for the reflection coefficient [[29], which in the case of normal plane-wave incidence is given by

$$V = \frac{sh\left[\frac{\pi^2 \Delta h}{2\lambda} \cdot \left(1 - \sqrt{1 - 2\Delta c/c}\right)\right]}{sh\left[\frac{\pi^2 \Delta h}{2\lambda} + \sqrt{1 - 2\Delta c/c}\right]}, \quad (4)$$

Frequency dependences of reflection from the sand–clay transition layer of the effective thickness Δh = 10 mm at different temperatures (Figure 8b) show that the reflection coefficient increases for both frequencies from +2 °C to −10 °C cooling: 0.27 to 0.5 at 50 kHz and 0.01 to 0.15 at 200 kHz.

Thus, simple modeling shows that reflection from a layered feature increases markedly upon its cooling from +2 to −10 °C due to the roughness of interfaces and nonzero thicknesses of the intermediate layer. The echo duration Δ increases correspondingly.

3.2.2. Temperature Dependence of the Attenuation of Acoustic Waves in Bottom Sediments

The attenuation of acoustic waves in bottom sediments, the other factor that controls the echo duration Δ, is likewise sensitive to temperature. Calculations and laboratory experiments on various natural marine sediments [29–32] showed that the attenuation of high-frequency acoustic waves is almost independent of positive temperatures [29,30] but shows strong temperature dependence at subzero and negative temperatures [32] (Figure 9). Calculations for 1 MHz [31] show that waves in the sand attenuate for two orders of magnitude upon cooling from +2 °C to −15 °C, and the attenuation coefficient approaches the values of pure ice. This prominent temperature dependence of the attenuation coefficient and the sound velocity is due to the decrease in viscous friction as free water becomes bound [33] and a part of pore moisture freezes up to ice [31].

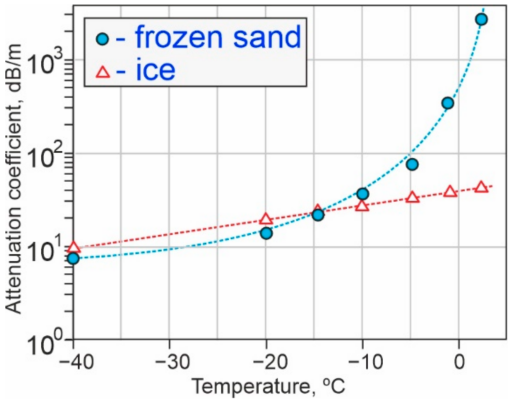

Figure 9. Temperature dependence of ultrasound attenuation (1 MHz) in frozen sand and ice modified from [31].

3.3. Discussion

Echo sounding surveys in the eastern Arctic shelf at frequencies of 50 and 200 kHz showed that echo duration Δ correlates with the temperature of shallow bottom sediments and generally increases as the sediments become colder below 0.5 °C. Note that the Δ values do not correlate with particle sizes in this temperature range ($T < T_0 = 0.5$ °C). As demonstrated by modeling, echo duration increases the account of reflection from layered features and decreases attenuation. It should be noted that the proposed model (Figures 7 and 8), based on a layered structure, is quite realistic since the sedimentary stratum of the seabed throughout the world ocean is characterized by a layered structure of various scales. This layering of the seafloor structure is due to variations in sedimentation associated with various processes and natural cycles, and it is a characteristic feature of echograms (see, for example, [34,35]).

The obtained temperature dependences of echo duration (trends in Figure 5) can make reference for remote estimation of sediment temperatures by high-frequency acoustic thermometry. In the approach we suggest, temperatures are estimated from echo duration Δ rather than from the travel time between the emitter and receiver as in the conventional long-range acoustic thermometry [33,36]. The durations of Δ > 4 ms measured by the described sonar system at frequencies 50 and 200 kHz will correspond to the sediment temperatures $T < T_0 = 0.5$ °C with 95% probability. The most probable temperature values can be estimated from Δ values using the trends in Figure 5.

This is a remote sensing method that does not require embedding transducers into sediments. Furthermore, the measurements are actually instantaneous as there is no need to wait for thermodynamic equilibrium between the sensor and the ambiance.

The high-frequency acoustic thermometry can be applied to large volumes of sediments beyond the upper 1 m layer. The covered volumes depend on the specifications of the sonar system, sounding frequency, attenuation, and operation conditions. Temperature measurements at frequencies of hundreds of kilohertz can provide real-time average seabed sediment temperature estimates while cruising, which is of great theoretical and practical significance. Specifically, the temperature data are important for monitoring the subsea permafrost and marine methane hydrates and for contouring the zones of hydrate dissociation or dense water cascading [37].

The method is the most sensitive in the temperature range from slightly above the freezing point of free liquid to the point when almost all pore water converts to ice. This is quite a large range, given that pore water commonly freezes up at lower temperatures than ordinary free water. For the greatest part of sediments, it is from +2 to −10 °C [31], the lower bound being dependent on the type of rocks and pore space patterns. Note that temperature measurements for any specific type of sediment should begin with finding the empirical relationship between the echo duration and the average temperature of shallow sediments in the target temperature range.

4. Conclusions

Echo sounding results from the Anadyr Gulf and the shelves of the East Siberian and Laptev seas have demonstrated that the duration of signal backscattered from the seabed (echo duration, Δ) recorded at frequencies of 50 and 200 kHz correlates with temperature and generally increases with cooling of sediments from >0.5 °C. This trend can be explained by modeling with a layered structure of bottom sediments.

The temperature dependence of echo duration values created a reference for a new method of remote high-frequency acoustic thermometry, in which they are used to infer the temperatures of shallow bottom sediments according to empirical relationships.

High-frequency acoustic thermometry has multiple applications: contouring of low-temperature zones, remote sensing of seabed temperatures, or estimating the thickness of frozen subbottom sediments, with implications for the location of subsea permafrost and stability of gas hydrates and consequent methane release in the Arctic shelf region.

Author Contributions: Conceptualization, V.Y., A.S., N.S. and I.S.; methodology, V.Y. and A.S.; software, V.Y., A.S. and D.C.; validation, V.Y. and A.S.; formal analysis, V.Y., A.S. and D.C.; investigation, V.Y. and A.S.; resources, N.S. and I.S.; data curation, V.Y., A.S. and D.C.; writing—original draft preparation, V.Y.; writing—review and editing, V.Y., A.S., N.S., D.C. and I.S.; visualization, V.Y., A.S., A.D. and D.C.; supervision, V.Y., I.S. and N.S.; project administration, I.S. and N.S.; funding acquisition, V.Y., I.S. and N.S. All authors have read and agreed to the published version of the manuscript.

Funding: The study was carried out at the Tomsk State University as part of Program *Prioritet 2030* run by the Ministry of Science and Education of the Russian Federation. A part of the work was performed under government assignment of the Federal Scientific Research Center *Crystallography and Photonics* and under Program 0211-2021-0010, all supported by the Ministry of Science and Education of the Russian Federation.

Institutional Review Board Statement: Not applicable.

Informed Consent Statement: Not applicable.

Data Availability Statement: Not applicable.

Acknowledgments: We wish to thank V. Balabashin, A. Voronin, O. Dudarev, and the crew of *RV* Nikolay Kolomeitsev for assistance with onboard work.

Conflicts of Interest: The authors declare no conflict of interest.

References

1. Parry, M.L. *Intergovernmental Panel on Climate Change. Climate Change 2007: Impacts, Adaptation and Vulnerability. Contribution of Working Group II to the fourth Assessment Report of the Intergovernmental Panel on Climate Change*; Cambridge University Press: Cambridge, UK, 2007.
2. Friedlingstein, P.; Cox, P.; Betts, R.; Bopp, L.; Von Bloh, W.; Brovkin, V.; Cadule, P.; Doney, S.; Eby, M.; Fung, I. Climate–carbon cycle feedback analysis: Results from the C4MIP model intercomparison. *J. Clim.* **2006**, *19*, 3337–3353. [CrossRef]
3. Gruber, N. Warming up, turning sour, losing breath: Ocean biogeochemistry under global change. *Philos. Trans. R. Soc. A -Math. Phys. Eng. Sci.* **2011**, *369*, 1980–1996. [CrossRef] [PubMed]
4. Koven, C.; Ringeval, B.; Friedlingstein, P.; Ciais, P.; Cadule, P.; Khvorostyanov, D.; Krinner, G.; Tarnocai, C. Permafrost carbon-climate feedbacks accelerate global warming. *Proc. Natl. Acad. Sci. USA* **2011**, *108*, 14769–14774. [CrossRef] [PubMed]
5. Soloviev, V.A.; Ginzburg, G.D.; Telepnev, E.V.; Mikhaluk, Y.N. *Cryothermia and Gas Hydrates in the Arctic Ocean*; Sevmorgeologia: Leningrad, Russia, 1987. (In Russian)
6. Kvenvolden, K. Methane hydrate and global climate. *Glob. Biogeochem. Cycles* **1988**, *2*, 221–229. [CrossRef]
7. Shakhova, N.; Semiletov, I.; Salyuk, A.; Yusupov, V.; Kosmach, D.; Gustafsson, O. Extensive methane venting to the atmosphere from sediments of the East Siberian Arctic Shelf. *Science* **2010**, *327*, 1246–1250. [CrossRef] [PubMed]
8. Shakhova, N.; Semiletov, I.; Leifer, I.; Sergienko, V.; Salyuk, A.; Kosmach, D.; Chernykh, D.; Stubbs, C.; Nicolsky, D.; Tumskoy, V.; et al. Ebullition and storm-induced methane release from the East Siberian Arctic Shelf. *Nat. Geosci.* **2014**, *7*, 64–70. [CrossRef]
9. Shakhova, N.; Semiletov, I.; Chuvilin, E. Understanding the permafrost–hydrate system and associated methane releases in the East Siberian Arctic Shelf. *Geosciences* **2019**, *9*, 251. [CrossRef]
10. Shakhova, N.; Semiletov, I.; Leifer, I.; Rekant, P.; Salyuk, A.; Kosmach, D. Geochemical and geophysical evidence of methane release from the inner East Siberian Shelf. *J. Geophys. Res.* **2010**, *115*, C08007. [CrossRef]

11. Shakhova, N.E.; Nicolsky, D.Y.; Semiletov, I.P. Current state of subsea permafrost on the East Siberian Shelf: Tests of modeling results based on field observations. *Dokl. Earth Sci.* **2009**, *429*, 1518–1521. [CrossRef]
12. Romanovskii, N.N.; Hubberten, H.W. Results of permafrost modelling of the lowlands and shelf of the Laptev Sea region, Russia. *Permafr. Periglac. Process.* **2001**, *12*, 191–202. [CrossRef]
13. Nicolsky, D.J.; Romanovsky, V.E.; Romanovskii, N.N.; Kholodov, A.L.; Shakhova, N.E.; Semiletov, I.P. Modeling subsea permafrost in the East Siberian Arctic Shelf: The Laptev Sea region. *J. Geophys. Res. Earth Surf.* **2012**, *117*, 22. [CrossRef]
14. Shakhova, N.; Semiletov, I.; Gustafsson, O.; Sergienko, V.; Lobkovsky, L.; Dudarev, O.; Tumskoy, V.; Grigoriev, M.; Mazurov, A.; Salyuk, A.; et al. Current rates and mechanisms of subsea permafrost degradation in the East Siberian Arctic Shelf. *Nat. Commun.* **2017**, *8*, 15872. [CrossRef] [PubMed]
15. O'Regan, M.; Preto, P.; Stranne, C.; Jakobsson, M.; Koshurnikov, A. Surface heat flow measurements from the East Siberian continental slope and southern Lomonosov Ridge, Arctic Ocean. *Geochem. Geophys. Geosyst.* **2016**, *17*, 1608–1622. [CrossRef]
16. Yusupov, V.I.; Salyuk, A.N.; Karnaukh, V.N.; Semiletov, I.P.; Shakhova, N.E. Detection of methane ebullition in shelf waters of the Laptev Sea in the Eastern Arctic Region. *Dokl. Earth Sci.* **2010**, *430*, 261–264. [CrossRef]
17. Ananiev, R.A.; Dmitrevsky, N.N.; Roslyakov, A.G.; Chernykh, D.V.; Moroz, E.A.; Zarayskaya, Y.A.; Semiletov, I.P. Acoustic monitoring of gas emission processes in the Arctic Shelf Seas. *Oceanology* **2022**, *62*, 127–132. [CrossRef]
18. Zhao, J.; Mai, D.; Zhang, H.; Wang, S. Automatic detection and segmentation on gas plumes from multibeam water column images. *Remote Sens.* **2020**, *12*, 3085. [CrossRef]
19. Chernykh, D.; Yusupov, V.; Salomatin, A.; Kosmach, D.; Shakhova, N.; Gershelis, E.; Konstantinov, A.; Grinko, A.; Chuvilin, E.; Dudarev, O.; et al. Sonar estimation of methane bubble flux from thawing subsea permafrost: A case study from the Laptev Sea shelf. *Geosciences* **2020**, *10*, 411. [CrossRef]
20. Shakhova, N.; Semiletov, I.; Sergienko, V.; Lobkovsky, L.; Yusupov, V.; Salyuk, A.; Salomatin, A.; Chernykh, D.; Kosmach, D.; Panteleev, G.; et al. The East Siberian Arctic Shelf: Towards further assessment of permafrost-related methane fluxes and role of sea ice. *Philos. Trans. R. Soc. A -Math. Phys. Eng. Sci.* **2015**, *373*, 20140451. [CrossRef] [PubMed]
21. Snellen, M.; Gaida, T.C.; Koop, L.; Alevizos, E.; Simons, D.G. Performance of multibeam echosounder backscatter-based classification for monitoring sediment distributions using multitemporal large-scale ocean data sets. *IEEE J. Ocean. Eng.* **2019**, *44*, 142–155. [CrossRef]
22. Shang, X.; Zhao, J.; Zhang, H. Obtaining high-resolution seabed topography and surface details by co-registration of side-scan sonar and multibeam echo sounder images. *Remote Sens.* **2019**, *11*, 1496. [CrossRef]
23. Jakobsson, M.; Nilsson, J.; Anderson, L.; Backman, J.; Bjork, G.; Cronin, T.M.; Kirchner, N.; Koshurnikov, A.; Mayer, L.; Noormets, R.; et al. Evidence for an ice shelf covering the central Arctic Ocean during the penultimate glaciation. *Nat. Commun.* **2016**, *7*, 10365. [CrossRef] [PubMed]
24. Nosov, A.V.; Postnov, G.A. Measurement of the acoustic parameters of the ocean bottom using multiply scattered sound pulses. *Acoust. Phys.* **2001**, *47*, 448–451. [CrossRef]
25. Shakhova, N.; Semiletov, I. Methane release and coastal environment in the East Siberian Arctic shelf. *J. Mar. Syst.* **2007**, *66*, 227–243. [CrossRef]
26. Brekhovskikh, L.M.; Godin, O.A. *Acoustics of Layered Media*; Nauka: Moscow, Russia, 1989. (In Russian)
27. Bjørnø, L.; Neighbors, T.; Bradley, D. *Applied Underwater Acoustics: Leif Bjørnø*; Elsevier: Amsterdam, The Netherlands, 2017; pp. 1–964.
28. Brekhovskikh, L. *Waves in Layered Media*; Elsevier Science: Amsterdam, The Netherlands, 2012.
29. Bell, D.; Shirley, D. Temperature variation of the acoustical properties of laboratory sediments. *J. Acoust. Soc. Am.* **1980**, *68*, 227–231. [CrossRef]
30. Shirley, D. Temperature variation of the acoustic properties of laboratory sediments. *J. Acoust. Soc. Am.* **1979**, *66*, S45–S46. [CrossRef]
31. Frolov, A.D. *Electrical and Elastic Properties of Frozen Rocks and Ice*; Russian Academy of Sciences: Moscow, Russia, 2005. (In Russia)
32. Wang, D.-Y.; Zhu, Y.-L.; Wei, M.; Niu, Y. Application of ultrasonic technology for physical–mechanical properties of frozen soils. *Cold Reg. Sci. Technol.* **2006**, *44*, 12–19. [CrossRef]
33. Sabinin, K. Oceanological aspects of acoustic thermometry of the Arctic Ocean. *Usp. Fiz. Nauk* **1995**, *38*, 793. [CrossRef]
34. Schlager, U.; Jokat, W.; Weigelt, E.; Gebhardt, C. Submarine landslides along the Siberian termination of the Lomonosov Ridge, Arctic Ocean. *Geomorphology* **2021**, *382*, 107679. [CrossRef]
35. Blumenberg, M.; Lutz, R.; Schlömer, S.; Krüger, M.; Scheeder, G.; Berglar, K.; Heyde, I.; Weniger, P. Hydrocarbons from near-surface sediments of the Barents Sea north of Svalbard–indication of subsurface hydrocarbon generation? *Mar. Petrol. Geol.* **2016**, *76*, 432–443. [CrossRef]
36. Worchester, P.; Dzieciuch, M.; Sagen, H. Ocean acoustics in the rapidly changing Arctic. *Acoust. Today* **2020**, *16*, 55–64. [CrossRef]
37. Chuvilin, E.; Bukhanov, B.; Yurchenko, A.; Davletshina, D.; Shakhova, N.; Spivak, E.; Rusakov, V.; Dudarev, O.; Khaustova, N.; Tikhonova, A.; et al. In-situ temperatures and thermal properties of the East Siberian Arctic shelf sediments: Key input for understanding the dynamics of subsea permafrost. *Mar. Petrol. Geol.* **2022**, *138*, 105550. [CrossRef]